Small-Angle X-ray Scattering Characterization of Agarose Sols and Gels

M. Djabourov*,†

Ecole de Physique et Chimie, 10 Rue Vauquelin, 75231 Paris Cedex 05, France

A. H. Clark, D. W. Rowlands, and S. B. Ross-Murphy

Unilever Research Laboratory, Colworth House, Sharnbrook, Bedford MK44 1LQ, U.K.
Received March 23, 1988; Revised Manuscript Received June 20, 1988

ABSTRACT: The structures of agarose sols and gels have been investigated by small-angle X-ray scattering (SAXS). Different concentrations and thermal treatments of the solutions have been explored. For the gels the angular distribution of the scattered intensity is consistent with a model based on a fibrous structure containing rodlike fibers of variable thickness. The probability density function for rod diameter has not been established, but there is evidence that a substantial subpopulation of thin rods is present and that these have an average diameter of ~30 Å. A molecular description of agarose chain association consistent with the SAXS measurements for the gel and based on the 12-chain hexagonal rod structure (~30-Å diameter) is discussed. Observations from polarimetry and optical microscopy are briefly reported, and possible interpretations of the results in terms of gelation and gel-melting mechanisms are given.

Introduction

Agarose is the major component of commercial agar, a polysaccharide extracted from marine red algae (*Rhodophyceae*). Agarose gels have a number of practical uses: for example, in laboratory work they act as bacterial culture supports and as separation media in column chromatography. They are also employed in medicine and in pharmacy, and in the food industry agar serves as a thickening and gelling ingredient. Like gelatin, agarose forms a thermoreversible gel in aqueous solution, but there is the significant difference that the range of thermal stability of the agarose gel is much greater than that of gelatin. The setting temperature is usually close to 40 °C, while the melting temperature is considerably higher (around 90 °C). Note that here both "setting" and "melting" represent simple observational concepts and are not rigorously identifiable with the normal scientific meanings of these terms.

Agarose gels have very high elastic moduli at low concentrations (e.g., $\sim 10^6$ dyn cm^{-2} at a few percent w/w concentration in contrast to, for example, gelatin gels, which usually require a concentration of around 30% w/w or more to achieve the same order of rigidity), and they are brittle and distinctly turbid (grayish appearance). In the present paper the molecular structure of agarose gels, i.e., network structure, is of particular concern together with details of the molecular mechanism of gelation. First, however, a review is given of what is already known about agarose as a biopolymer and about the process of gelation of this material.

Ideally, agarose is a linear copolymer[1,2] composed of alternating 1,3-linked β-D-galactopyranose (residue A) and 1,4-linked 3,6 anhydro-α-L-galactopyranose (residue B) as shown in Figure 1. However, a variable proportion of the β-D-galactose residues can be found substituted by sulfate or O-methyl groups at the 6-position, and the anhydride can be substituted by sulfate, O-methyl, or pyruvate groups at the 2-position. The amount of such substitution is known to modify the physical properties of the gels.[1-3] In addition the chain may also deviate from the ideal form of Figure 1 by having some of the 3,6-dihydro-α-L-galactose replaced by galactose or by galactose 6-sulfate,[4] an effect that breaks the natural sequence. It has been widely suggested that such spurious residues have a role to play in network formation as they prevent perfect ordering of chains and consequent crystallization and precipitation.[5-7]

At present there is no universal agreement about the mechanism of gelation of agarose. Studies have been made both of the dilute aqueous gels and of fibers prepared from them by dehydration and stretching. This work was suggested that an agarose coil-to-double helix transition is the origin of the gelation process. This picture emerges particularly from studies of oriented fibers by Arnott et al.[3] using X-ray diffraction. The double helix proposed (Figure 2) is able to accommodate substituents such as sulfate and pyruvate groups and is a left-handed 3-fold helix, with a pitch of 19 Å. The agarose gel network is described as arising both by double helix formation and by subsequent aggregation of these helices into bundles (see also Figure 2).

Another technique that has provided information about the gelling process is optical rotation.[8] This chiroptical spectroscopic approach is widely used to monitor the conformational states of biopolymers since it is often sensitive to changes in the molecular environment of each and very individual polymer residue, particularly when such changes are produced by variations in local interresidue angles of torsion.[9] There are practical limitations, however, and here for agarose, on account of turbidity, only studies of very dilute solutions are possible (e.g., less than 0.2% w/w). Where such work has been done, it turns out that the sign and magnitudes of the changes in optical rotation produced as such solutions are cooled are consistent with the geometry proposed for the double helix by fiber diffraction.[3,9] In addition, the large hysteresis loop observed when optical rotation is monitored during both the cooling and heating steps has been interpreted as indicating that a substantial amount of helix aggregation accompanies the network-building process.[3]

The structure of agarose gels at longer range is less well characterized. Only a few papers deal with the supramolecular structure in the gel state. In light scattering[10] performed in extremely dilute solutions at room temperature ($C \leq 0.05\%$ w/w) the angular distribution of intensity corresponds to randomly oriented rodlike particles whose mass per unit length is estimated to be of the order $(1.2\text{–}1.7) \times 10^{-13}$ g cm^{-1}. The presence of a small number of larger aggregates is also mentioned, but these were not

† Work carried out while on sabbatical leave at the Unilever Research Laboratory, Colworth House, Bedford, U.K.

0024-9297/89/2222-0180$01.50/0

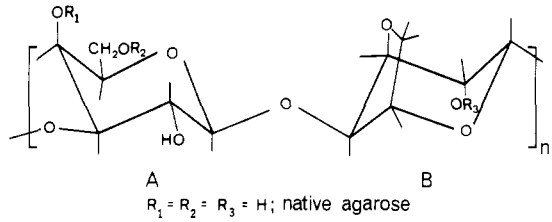

Figure 1. Idealized AB repeat unit of the agarose polymer: (A) 1,3-linked β-D-galactose residue; (B) 1,4-linked 3,6-anhydro-α-L-galactose residue.

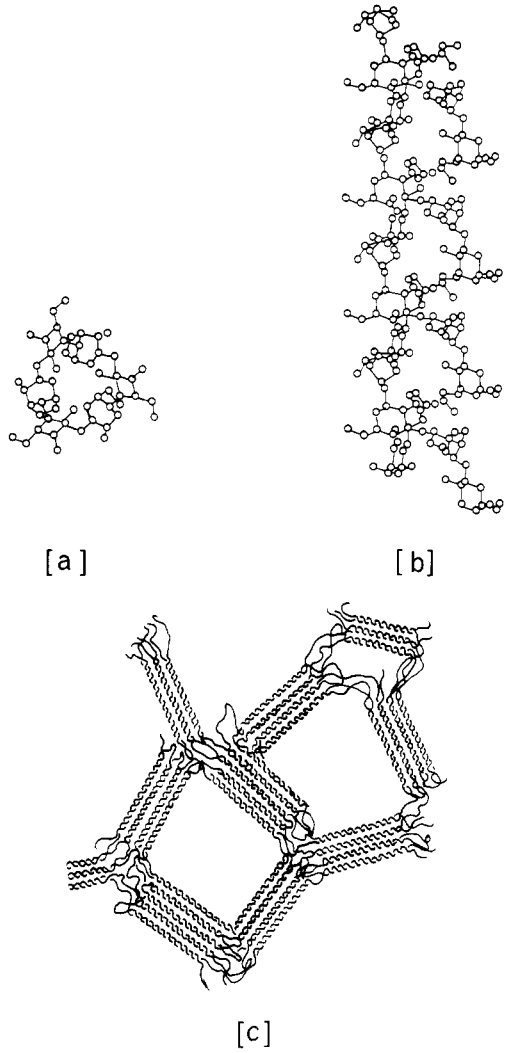

Figure 2. Structure of the agarose double helix (a and b) as proposed by Arnott et al.[3] A schematic representation of their model for the agarose gel network structure is also shown (c).

characterized. Working on pearl-condensed agarose gels (C = 2–8% w/w), Laurent[11] concluded from a gel chromatographic investigation that the gel network was constructed from fibers of diameter ≃50 Å.

A somewhat different description has been reported by Pines and Prins.[12] Light scattering from systems containing agarose at concentrations in the range 0.5–1.0% w/w and at temperatures of 30–40 °C showed a distinct maximum ($h = 6 \times 10^{-5}$ Å^{-1} for C = 1% w/w), and the authors concluded that gel formation was driven by a spinodal decomposition mechanism. In support of this interpretation they stated that "closely packed spherical regions of the order of a few times 10000 Å" were observable in the optical microscope, i.e., a phase-separated system was involved. In this context it is interesting that gelation of biopolymers by a spinodal decomposition mechanism has also been proposed by Miller and coworkers and extensively discussed by them.[13]

It is the aim of the current investigation of agarose gelation to clarify the mechanism of network formation and to determine whether different mechanisms and structures result as gelling conditions are changed. To these ends the gel network has been characterized at various concentrations and after various thermal treatments, using small-angle X-ray scattering (SAXS) (Kratky camera) applied over a range of scattering vectors: 1.5×10^{-2}–3.5×10^{-1} Å^{-1}. Experimental details are described first, results are then presented and analyzed, and finally a microscopic model of the structure of the network is proposed. This is in agreement with the interpretation of the scattering curves and incorporates previous ideas about the molecular structure of junction zones.

Experimental Section

The agarose sample was supplied as a high-quality bacteriological agar. This meant that it was likely to show only small degrees of imperfection in relation to the ideal repeat formula of Figure 1. Analytical figures showed that the sulfate content was of the order of 0.7% and pyruvate 1.90% while calcium (33 ppm) and magnesium (13 ppm) were also detected. It should be noted that divalent cations can crucially influence the gelation of polysaccharide polymers (e.g., alginates, carrageenans),[14] particularly where charged groups (carboxylate, sulfate) are present. In the case of agarose, however, such effects are expected to be much less important on account of the essentially neutral nature of this biopolymer. Chromatographic studies showed that polydispersity of the present sample was 3.3 and the average molecular weight M_w = 512000.[15]

Solutions of agarose in deionized water were made up by heating mixtures in a pressure vessel to 120 °C for 15–20 min. This treatment is apparently sufficient to ensure complete dissolution (see below), and hot solutions were then filtered through Millipore filters of porosities ranging from 1.2 to 0.22 μm to eliminate dust particles. Other methods of sample preparation explored included treatment at 100 °C for 20–25 min using a steam bath. However, this procedure failed to ensure complete dispersal of the agarose as some of the samples formed apparently clear solutions at high temperatures (~90–100 °C) but separated on cooling (40–50 °C). This material would not redissolve on sample agitation and was ascribed to incomplete dissolution of the agar on treatment at lower temperatures. This effect did not occur for the autoclaved samples, and subsequently the autoclaving procedure was adopted as standard.

Optical rotation measurements were made with a Perkin Elmer 241 MC digital polarimeter operating at wavelength 436 nm. The cells were thermostated, and the optical path selected was 10 cm. In the optical rotation work the agarose concentration was fixed at 0.5% w/w.

Small-angle X-ray scattering measurements were performed with a Kratky camera equipped with a CGR position-sensitive proportional X-ray detector coupled to a Canberra multichannel analyzer. The X-ray source was a Philips 1730 sealed-tube high-stability X-ray generator operating at the copper Kα wavelength (λ) of 1.54 Å. This equipment allowed scattered intensity to be measured over a range of scattering angles 2θ equivalent to values of the reciprocal space variable h running from $h = 1.5 \times 10^{-2}$ to 3.5×10^{-1} Å^{-1} ($h = 4\pi \sin \theta/\lambda$). These intensity measurements were not corrected for the error introduced by the slit-focused nature of the incident beam. Instead, theoretical curves were calculated to include the smearing error and were thus compared with the experimental data in an equivalent form. No attempt was made to perform absolute intensity measurements in the current investigation.

The agarose systems studied by small-angle X-ray scattering covered a wide range of concentrations (0.1–5% w/w), clear weak gels being obtained at the lowest polymer concentration and strong brittle turbid gels at higher concentrations. At 5% w/w, dissolution of agarose was difficult, the hot solutions obtained being highly viscous. This constrained the upper limit of concentration for such experiments.

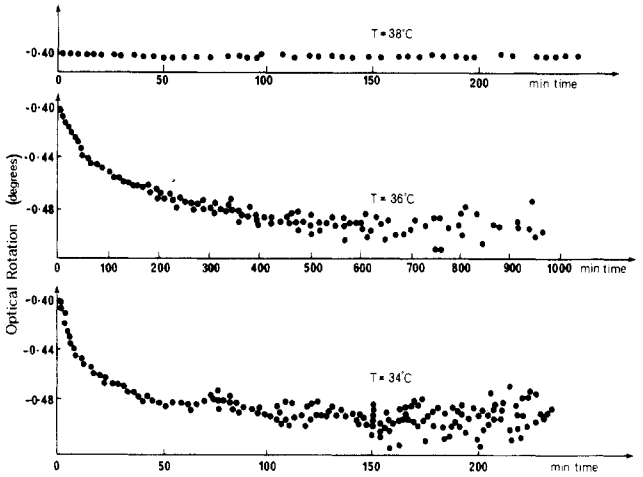

Figure 3. Time-dependence of the optical rotation measured at $\lambda = 436$ nm for hot agarose solutions initially at $T = 90$ °C, rapidly cooled to $T = 38$, 36, or 34 °C. The agarose concentration is 0.5% w/w.

Results

Optical Rotation. Polarimetry of 0.5% w/w agarose solutions was carried out to detect the temperature range of the conformational transition. This was a necessary preparation for further small-angle X-ray scattering measurements over the same temperature interval. Hot solutions (~90 °C) were cooled to temperatures $T = 38$, 36, or 34 °C, and the time dependence of optical rotation change was monitored. Results appear in Figure 3. No change occured at 38 °C even after 4 h. At lower temperatures the observed change begins soon after the lower temperature is reached, but the overall magnitude of the change is small (–0.4 to –0.5°). The effect is temperature dependent, the time to equilibration varying from 1 to 3–4 h. Gelation itself inhibits the measurement procedure since the reduction in transmitted light it produces falls below 50%. It turns out that optical rotation cannot be used systematically for samples of higher concentrations or over the full temperature range. SAXS was seen as a more versatile approach to the problem.

SAXS Measurements. SAXS can be used to characterize both sol and gel. There are limitations imposed by the necessity to accumulate data from weakly scattering samples. An hour was usually required in the present case and sometimes longer for very dilute samples. As a result, behavior faster than a scale of hours could not be followed, and this was particularly limiting during the setting of the gels. Nevertheless, long-time effects could be determined.

Figure 4 presents scattering data for sol (~90 °C) and gel (25 °C) for a 2.4% agarose system. Here scattered intensity is plotted as a function of scattering vector h between 0.015 and 0.35 Å^{-1}. The data have been corrected by subtracting scattering contributions from the holder and the aqueous solvent and normalizing the residual for exposure time and polymer concentration. The difference in scattering between sol and gel is very large and at once demonstrates that gelation involves the production of much larger molecular species than were present initially. Further experiments were performed, some on preset gels containing different levels of agarose and some involving the determination of hysteresis loops in a manner analogous to the optical rotation studies. These are now described.

Isothermal Gelation. The agarose concentrations considered were 0.1, 0.3, 0.6, 1.2, 2.4, and 5% w/w where gels were concerned, while only the 2.4% system was investigated in the hot sol state. Hot solutions were poured into the X-ray tubes, which were then sealed with grease and immediately plunged into a temperature-controlled bath. Four gelation temperatures were considered (34, 25, 15, and 4 °C), and samples were allowed to gel for 1-h minimum time, after which they were examined by SAXS at various intervals of time, between hours and 1 month. The results obtained can be summarized as follows:

(a) For most of the samples no time dependence of the scattered intensity curves was noticed, provided that 1–2 h were allowed for initial setting. For the most dilute samples (0.1 and 0.3% w/w) gelled above 4 °C, the first measurements were done only after ca. 24 h.

(b) For the fully set gels no dependence of the scattered intensity on thermal history was detected despite the variations in gelling conditions just described.

(c) The intensity usually scaled exactly with concentration over the whole range of scattering vectors ($h >$ 0.015 Å^{-1}) accessed. When differences between scaled curves were detectable, the shape of the scattering curves was not altered, only the overall amplitude (maximum difference in measured amplitude was ~20%). This is likely to have been a consequence of some drift in main beam intensity over the experimental period. Curves obtained for the dilute systems were of course much noisier, i.e., statistics were much poorer at the lower concentrations.

Because of the small effect of temperature, time, and concentration on the scattered intensity data from agarose gels under the prevailing conditions, we may consider the example in Figure 4, bottom, as typical of the gel state.

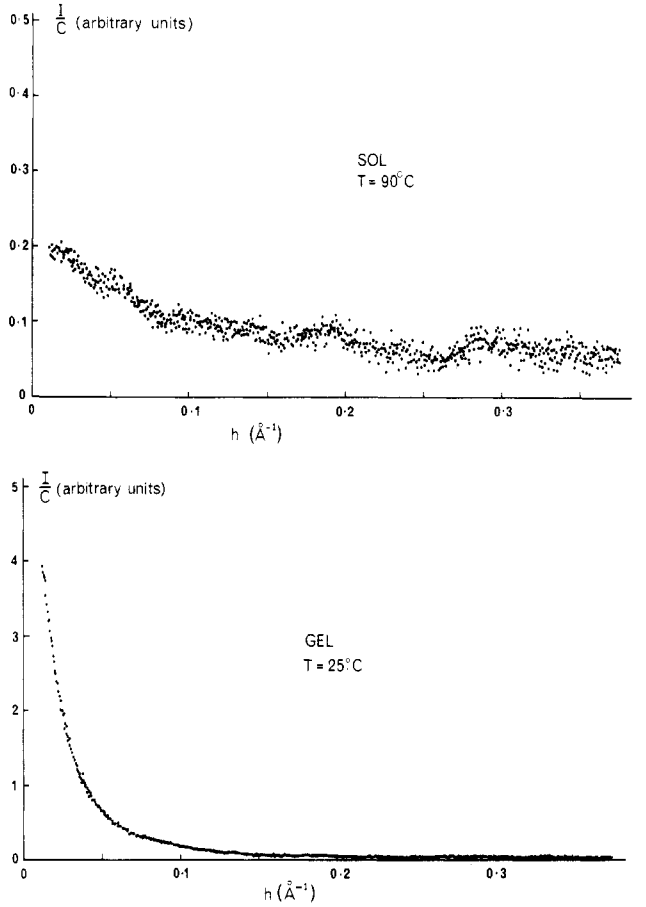

Figure 4. Top: angular dependence of the SAXS intensity from the sol state at $T = 90$ °C. Bottom: angular dependence of the SAXS intensity from the gel state at $T = 25$ °C. In both cases the agarose concentration is 2.4% w/w. The exposure times were 2 h for the sol and 1 h for the gel. Both data sets have been normalized with respect to polymer concentration and exposure time. Fluctuations apparent in the sol scatter curve arise from low intensity of signal and counter imperfections.

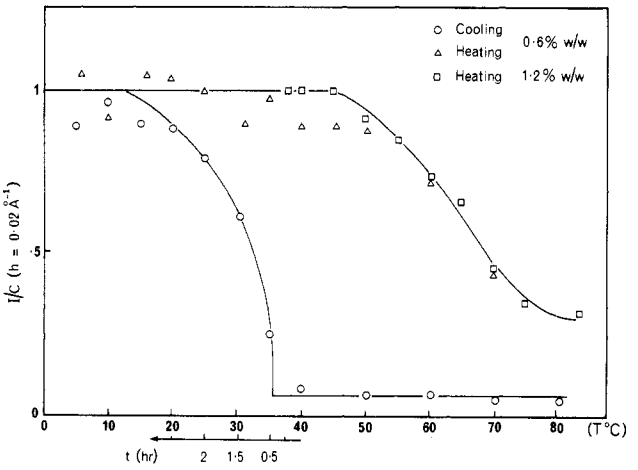

Figure 5. Hysteresis loop (○, △) for SAXS (one h value only) from an agarose solution of concentration 0.6% w/w. Temperature is changed by 5 °C every 0.75 h. Exposure time is 30 min. Also shown is melting curve (□) for a 1.2% w/w gel formed originally at room temperature. Here the exposure time was 1 h, and the rate of temperature change was 5 °C every 30 h.

Within the precision of the measurements the results indicate that the structure that develops after 1 or 2 h does not change further. Over the whole range of concentration certain features of the structure are evidently identical. This is a point that will be taken up again in later discussion.

Hysteresis Loops. SAXS was also used to study hysteresis effects during temperature cycles. Two concentrations were chosen, 0.6% and 1.2% w/w. The range of temperature explored was from 90 to 4 °C and was accessed first by cooling and then by heating. The rate of temperature change was 5 °C per 0.75 h, which includes an exposure time for X-rays of 0.5 h. The hysteresis loop obtained for the 0.6% sample is shown in Figure 5 and represents the intensity measured at a given value of h (h = 0.02 Å^{-1}) normalized to unity at the lowest temperatures (T < 10 °C) and displayed as a function of temperature. At the end of the cooling curve, the sample was maintained for 15 h at 4 °C before the heating period (duration 8 h) commenced. The following conclusions were reached:

(a) There is a distinct temperature gap between setting and melting. (Corresponding behavior has been observed in optical rotation vs temperature experiments[4-6] and shear modulus–temperature traces; see the Discussion.)

(b) Below T = 35 °C, by consideration of the time scale of the experiments in relation to the temperature scale, it may be deduced that the apparent temperature dependence of the cooling curve is actually due to the time required for equilibration (of the order of 2 h at T < 35 °C).

(c) Melting is still not complete at T = 70 °C, which shows the extreme stability of the low-temperature structure.

To check if any kinetic effects are present during the heating phase, we repeated the melting experiment using a concentration of 1.2% w/w, the exposure time being 1 h to achieve greater accuracy. The data obtained are also included in Figure 5. In this experiment the temperature was raised by 5 °C every 30 h, and the overall melting process was found to take place over 10 days! The slow-melting data are virtually identical with the rapid-melting measurements and hence the "molecular melting" involved is not under kinetic control. As Figure 5 also shows, the overall accuracy is significantly improved as the polymer concentration is increased and the data are accumulated over a longer period. The gel is apparently still not melted completely at 85 °C, which gives a melting temperature range between 45 and 90–100 °C, i.e., a width of approximately 50 °C. By contrast, the gelation process occurs quite sharply at 35 ± 1 °C. Overall, there is apparently no way of narrowing the gap between the gelling and melting temperatures, and this is in accordance with optical rotation results.

Theoretical Analysis

SAXS from a solution usually arises[16] from sources such as (i) individual particle scattering and (ii) interference of the scattering from these particles. The interference effect increases in importance as the particle concentration increases and, consequently, scattering experiments performed at different particle concentrations are required if these two effects are to be separated. Concentration effects, particularly excluded-volume effects, tend to contribute mainly at the lowest scattering vectors, provided that comparatively dilute solutions are being studied, and in this case interference effects can be assumed absent in the higher range of scattering angles: To an approximation the limit of scattering vector beyond which the interference effect becomes negligible is given by[17]

$$h^* > 5/D \quad (1)$$

where D is the maximum dimension of the particle concerned. Beyond this, the internal structure of the individual particles can be explored.

In the present case of agarose gels, since the scattered intensity scales with concentration over the accessible h vector range and since this scaled intensity is also comparatively independent of gel thermal history, it may be concluded that essentially only a local, i.e., essentially short-range, structural feature is being explored. In one sense this is entirely to be expected since the lowest value of h accessible in the current experiments was 0.015 Å^{-1}, and this means that the maximum dimension of elements of the gel structure directly measureable by the SAXS approach was only a few hundred angstroms (certainly no greater than 300 Å). What is perhaps less expected is that the gel structure even at this local level is not to some extent influenced by the concentration and thermal factors already mentioned. Changes in supramolecular structure, for example, not directly measurable by the X-ray technique might be indirectly detectable through associated local effects such as changes in network strand thickness and proximity. For the agarose gels studied here, however, this does not seem to be the case.

For a further interpretation of the current data it was necessary to make some assumption about the shape of the scattering elements in the sol and in the gel network. In the sol state, the dissolved macromolecules are expected to be present in so-called coil conformations though the fact that the estimated characteristic ratio C_∞ for macromolecules of the agarose type is around 45[18] warns that even at high temperatures these coils are to an extent stiffened and persistent. In other words, within a certain range of scattering vectors the scattering from these polymers should be consistent with rodlike character. From the data available, however (2.4% solution only), it was not possible to estimate the persistence length or to carry this analysis further. Where the gel network is concerned, electron micrograph[19] evidence already suggests a structure composed of rodlike fibers much thicker than would be expected for the coils in solution. It follows that rod structures of varying thicknesses and of lengths considerably in excess of 300 Å (the persistence lengths of typical multiple-helical polysaccharides, e.g., xanthan,[20] schizophyllan,[21] lie in the range 1200–1500 Å) provide a good starting point in any attempt to model the network

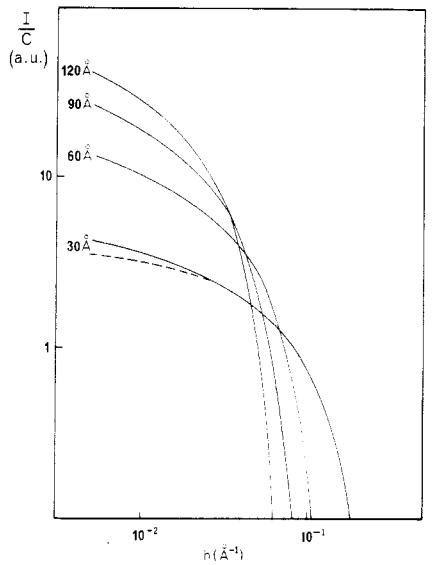

Figure 6. Computed SAXS intensities for rods of different cross sections (diameters as indicated) and same length ($2L$ = 1000 Å). The dotted line indicates the change in scattered intensity as a 30-Å rod gets shorter (i.e., when $2L$ = 300 Å and $2R$ = 30 Å). The smearing effects due to the Kratky camera are included in the computation.

scattering. This was the procedure adopted in the present work.

The angular distribution of the intensity scattered by a cylinder of diameter $2R$ and length $2L$ randomly oriented in relation to the X-ray beam has the form[22]

$$I(h) \propto (\rho - \rho_0)^2 V^2 \times \int_0^{\pi/2} \frac{\sin^2 (hL \cos \theta')}{h^2 L^2 \cos^2 \theta'} \frac{4J_1^2(hR \sin \theta')}{h^2 R^2 \sin^2 \theta'} \sin \theta' \, d\theta' \quad (2)$$

Here $(\rho - \rho_0)$ is the difference in average electron density between the particles ρ and the solvent ρ_0, V is the rod volume, θ' defines the angular orientation between the rod axis and the scattering vector, and J_1 is the first-order Bessel function. With the above equation the intensity distributions scattered by rods of different cross sections and lengths have been calculated, some results being shown in Figure 6. As mentioned earlier these theoretical curves contain the "smearing effect" appropriate to the experimental Kratky slit-focus main beam profile, this being introduced by convoluting the intensity $I(h)$ of eq 2 with the experimental trapezoidal distribution of main beam intensity in the registration plane, $W(z) \boxtimes W(h)$, i.e.

$$I(h)_{\text{smeared}} = \int_{-\infty}^{\infty} I(h^2 + z^2)^{1/2} \, W(z) \, dz \quad (3)$$

In Figure 6 results appear for rods of equal lengths (1000 Å) and diameters ranging from 30 to 120 Å. The intensity distributions in Figure 6, it should be noted, have been scaled according to particle volume so that they are appropriate to the scattering from unit mass of rod material, i.e., the reduction in numbers of particles which accompanies an increase in volume has been accounted for. It is also demonstrated in Figure 6 that if the rod length is reduced to, e.g., $2L$ = 300 Å, the slope of the inner part of the scattering function is modified ($h < 0.015$ Å), but this part of the function is not accurately determined by our experiment. It follows that the experiment is much more sensitive to changes in rod cross section than it is to length changes. It is evident that increasing rod diameter shifts the bulk of the scattering to smaller angles and increases the amplitude of scattering. This effect is particularly clear in the log–log representation of Figure 6,

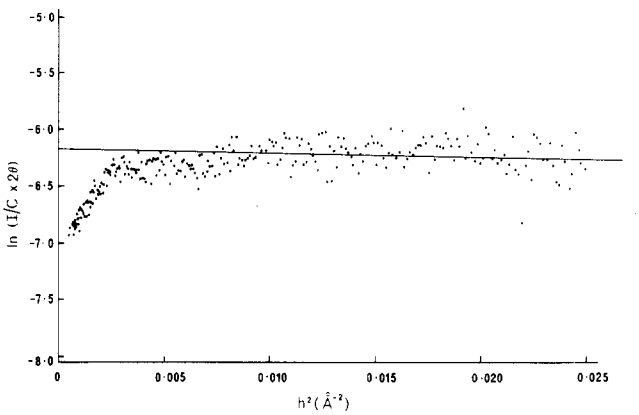

Figure 7. Cross-sectional plot of the scatter curve from the hot agarose solution. The slope of the fitted straight line corresponds to R_c = 2.6 (±0.8) Å.

where horizontal and vertical scalings are realized by simple translations.

In the limit of longs rods ($L \gg R$) the intensity scattered per particle can be separated into two components[16] (factors), one corresponding to the length effect and one to the rod cross section, i.e.

$$I(h) \propto (\rho - \rho_0)^2 (L/h) R_c^4 \exp(-h^2 R_c^2/2) \quad (4)$$

Here R_c is the radius of gyration of the rod cross section, or the root-mean-square distance of electron mass, from the rod axis. For a uniform rod of radius R the cross-sectional radius of gyration R_c is given by

$$R_c = R/2^{1/2} \quad (5)$$

The above approximation is valid for the observable low-angle parts of the rod scattering curves and suggests that a plot of log (Ih) (or log ($I2\theta$)) versus h^2 will contain a linear (cross-sectional Guinier) region whose slope is equal to $R_c^2/2$.

In the present work this method of plotting agarose scattering data was adopted as a means of extracting a measure of structure. Figure 7 shows what is obtained in the case of the sol scattering curve. Here it may be seen that in the h vector range $0.01 < h^2 < 0.025$ Å^{-2}, a linear portion appears whose slope can be calculated by linear regression. The result is R_c = 2.6 ± 0.8 Å, giving a rod diameter of the order of $2R$ = 7.42 ± 2.0 Å. This is comparable to the thickness expected for a single polysaccharide chain, but the precision of the result is clearly limited by the weak scattering signal (high noise level) from the sol, and the smearing effect which shifts the value of the radius slightly. The result obtained is very similar to a corresponding value obtained for a lithium derivative of the structurally rather similar (but ionizable) marine polysaccharide ι-carrageenan.[23] By a similar approach to that described here we obtained the result R_c = 2.5 ± 0.8 Å. This finding indicates that in the hot autoclaved solution the agarose polymer may be (at least at the level of cross section) considered to be essentially totally disaggregated from any multistranded helical form. However, as this implies, we cannot unequivocally establish that all forms of molecular aggregation are absent in the hot solution. Evidence from precision light-scattering measurements on carrageenans suggests that in their case some aggregation still remains.[24]

Figure 8 presents the corresponding Guinier plot of the gel data. At least two linear regions may be seen. This at once suggests that the distribution of rod thicknesses in agarose gels is not only polydisperse but almost certainly multimodal (more than one major population of cross-sectional thicknesses present). The least-squares fitting

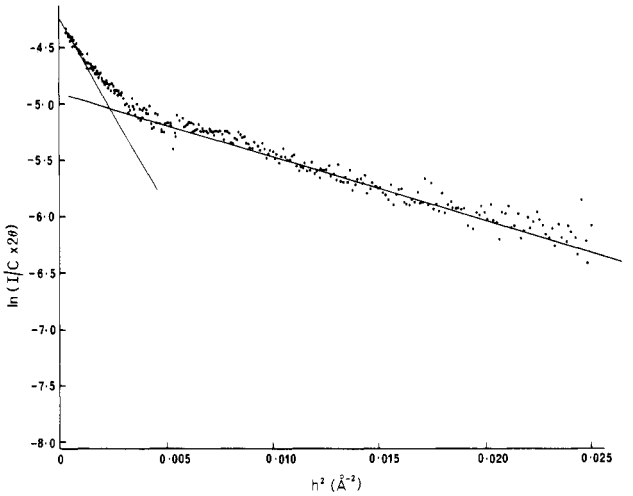

Figure 8. Cross-sectional plot of the scatter curve from the gel state. The slope of the innermost part gives R_c = 29 (±3) Å, and of the outermost part R_c = 10.4 (±1) Å.

procedure applied to the smaller h^2 range $2.3 \times 10^{-4} < h^2 < 9.0 \times 10^{-4}$ Å^{-2} gives a cross-sectional radius of gyration R_c of 29 ± 3.0 Å, which corresponds to rods of diameter (on average) $2R$ = 82 ± 8.0 Å. The same procedure for $1.0 \times 10^{-2} < h^2 < 3.0 \times 10^{-2}$ Å^{-2} gives R_c = 10.4 ± 1.0 Å, which is consistent with a rod diameter $2R$ = 29 ± 3.0 Å.

For confirmation of the above analysis, the theoretical scattering functions (smeared) for rods of diameters close to those suggested by the cross-sectional plots have been computed and compared with experiment. Thus two populations of rods have been assumed with average diameters equal to those extracted by Guinier plotting and the corresponding scattering functions added to reproduce the experimental observations. Results appear in Figure 9. Figure 9, top, shows the computed intensity curves assuming 30- and 90-Å diameters for the components. In this modeling exercise the rod lengths assumed were both 1000 Å. The relative amplitudes of the two contributions were adjusted to obtain best agreement with the experimental data (also shown). In Figure 9, bottom, the Guinier plot is given for the computed data and is again compared with experiment.

From these results it is clear that in agarose gels there is a strong dispersion of network strand thickness, and although the decomposition of the distribution into two distinct populations proposed above is almost certainly an over-simplification, the presence of a substantial subpopulation of thinner rods of around 30-Å diameter seems likely. These thinnest network strands determine total scattering from the gel over the range $0.093 < h < 0.17$ Å^{-1}, while at smaller h vectors, the larger species dominate. Here the fit to the two-population model is imperfect, indicating the limitations of the two-population description and the probable presence of species much larger in thickness than 90 Å. The two-population fit can be used, however, to provide a rough estimate of the proportion of thinnest species present. By weight, this model requires that there are 42% of the rods of 30-Å diameter and 58% of the 90-Å rods. On a number-average basis this means that there are ca. 7 times as many thin rods as there are thick ones if we make the reasonable assumption that this number can be inferred from the relative cross-sectional areas of the species involved. The prediction is that in electron micrographs, for example, mainly thin fibers should be observed, although with some larger ones present, and this is indeed the case.[19]

Turning to measures of agarose network structure achieved by other workers, it is of interest that for the

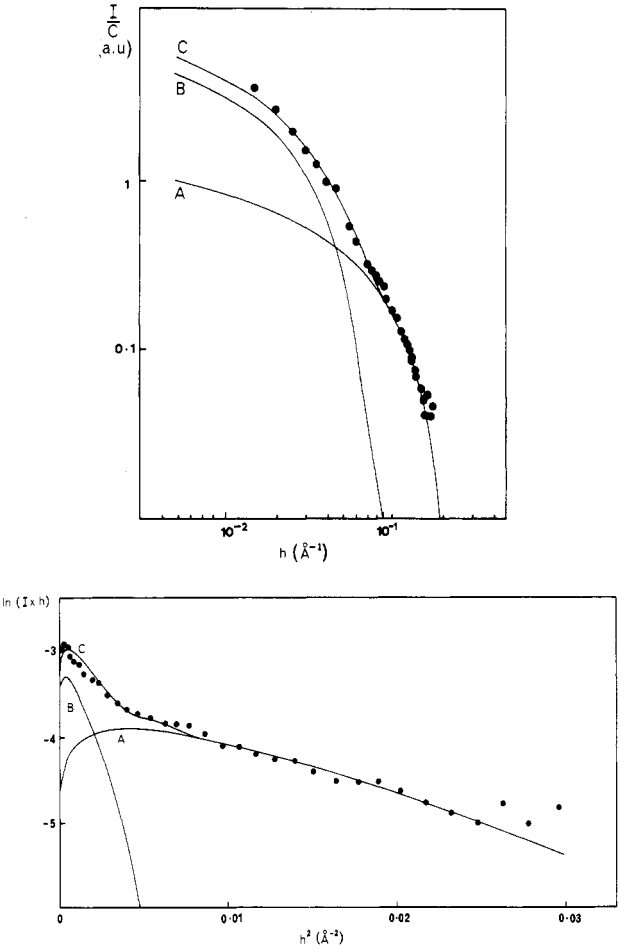

Figure 9. Top: computed intensities (smeared) for two populations of rods with diameters $2R$ = 30 Å (curve A) and $2R$ = 90 Å (curve B) and equal lengths ($2L$ = 1000 Å). The two contributions are added in curve C and compared with the experimental data (see text). Bottom: cross-sectional plots for the data in Figure 9, top.

thinner rods at least the current estimates of rod thickness are in reasonable agreement with an average diameter proposed by Laurent[11] from gel chromatography work, i.e., $2R \approx 50$ Å. They seem also to agree with the light-scattering investigation by Obrink[10] on very dilute systems ($C < 0.05\%$ w/w). This author proposed a value for the mass per unit length of the agarose aggregates present of $(1.2–1.7) \times 10^{-13}$ g cm^{-1}. An assumption must be made about the degree of hydration of the fibers to compare these figures with current findings. For pure agarose their density should be 1.6 g cm^{-3}, but for 50% hydration this reduces to say 1.3 g cm^{-3}. On this basis the 30-Å rods are expected to have a mass per unit length of $(1.13–1.0) \times 10^{-13}$ g cm^{-1} and the thick rods 1.0×10^{-12}–8.2×10^{-13} g cm^{-1}, which is an order of magnitude higher. However, in the light-scattering experiments larger aggregates were indeed noticed,[11] even though these were not accurately characterized.

In addition to the optical rotation and X-ray work, during the course of the current multitechnique investigation, agarose gels were also examined with the optical microscope (cross polars and phase contrast) to see if any large-scale structure could be observed, e.g., a cholesteric liquid crystal phase. Such features have been suggested already by Pines and Prins[12] for agarose gels and are of course also implicit in the Miller[13] model for biopolymer gel formation mentioned earlier. No such feature was observed for gels prepared at room temperature, however, and in the next section we return to microscopic consid-

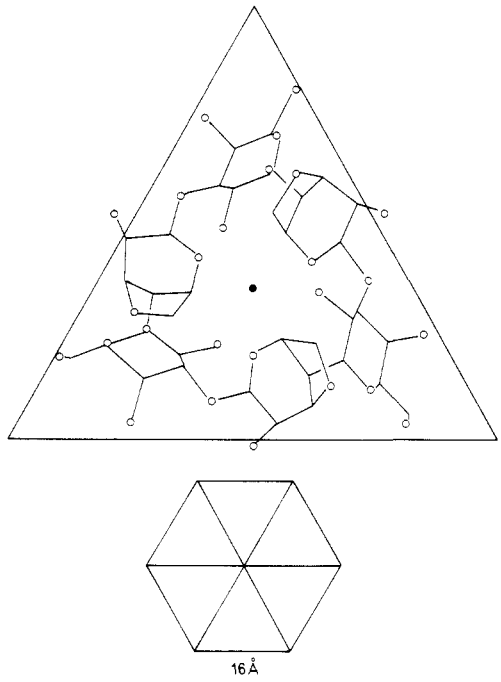

Figure 10. Projected structure of the agarose double helix (top) based on atomic coordinates from ref 3. Hexagonal fiber (in cross section) formed from six double helices is also indicated (bottom).

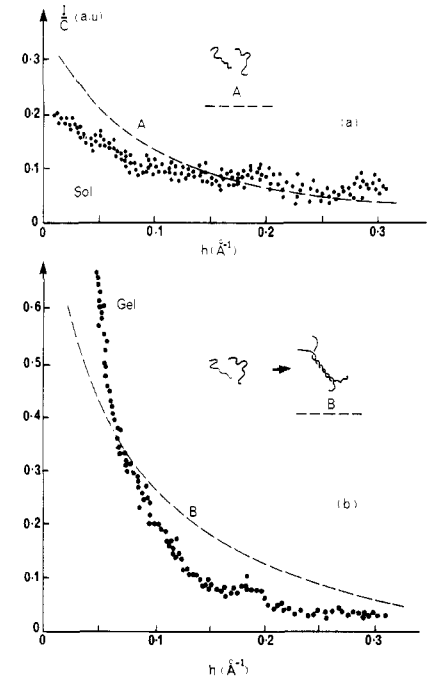

Figure 11. Calculated SAXS intensity (smeared) versus h curves for (a) the agarose single chain, and (b) the double helical conformation are compared with the experimental sol and gel scattering data. As the maximum measured intensity for the gel (Figure 4b) is ~4.0, formation of aggregates much thicker than the double helix is indicated.

erations and examine how the results of the current SAXS work may be related to conventional molecular descriptions of agarose network formation obtained, e.g., by fiber diffraction.

Although the SAXS technique cannot achieve atomic resolution and hence cannot comment precisely upon the conformation and mutual arrangement of polysaccharide chains in the fibers composing the gel, it is possible to assemble rodlike structures from the fiber-diffraction double helix, calculate a smeared scattering function, and compare this with the current experimental scattering data. Good agreement is then suggestive of a molecular interpretation, even though because of the nature of the SAXS experiment it can never prove conclusively that this is the only possible interpretation. In the present work, this method of modeling was attempted as a supplement to the purely homogeneous rod description.

Atomic coordinates for the agarose double helical structure were taken from the work of Arnott et al.[3] This helical arrangement is viewed in projection along the helix axis in Figure 10. To reduce computation when determining the X-ray scattering from this model, we idealized the sugar rings as point scatterers and computed the "residue" scattering (i.e., structure) factors $F_k(h)$ of such unit structures from the arrangement of atoms in the monosaccharide and their individual atomic scattering factors $f_i(h)$ (approximated as atomic numbers over the relevant h range). The equation used was the standard form:[22]

$$F_{\text{residue}}^2(h) = \sum_{i,j=1}^{\text{atoms/residue}} f_i f_j \frac{\sin(hr_{ij})}{hr_{ij}} \tag{6}$$

and the distributions of scattered X-ray intensity appropriate to a randomly oriented collection of single helices, double helices, etc., were computed by using the analogous result:

$$I(h) = \sum_{k,l=1}^{\text{residues/helix}} F_k F_l \frac{\sin(hR_{kl})}{hR_{kl}} \tag{7}$$

In eq 6 and 7 the quantities r_{ij} and R_{kl} are respectively distances between real atoms in individual sugar residues and distances between these residues (center-to-center) as they occur in the helical (or chain) structures. It should be noted that this approximation neglects any orientational property of the individual sugar residue scattering and approximates certain phase differences to zero. It is felt that the very similar nature of the residues concerned and their spherical character provide justification for these assumptions, especially when scattering at low angles only is to be considered.

The dependence of scattering on angle for the double helix calculated in the manner just described was, as anticipated, wholly unable to fit the experimental data for the gel (Figure 11b). This dependence was in fact more closely related to that obtained experimentally for the sol, a function that in turn could be modeled reasonably well (see Figure 11a) in terms of scattering calculable for a single agarose chain. In relation to this last calculation, however, it should be added that a single extended chain conformation alone was considered. This provided an approximation to the sol scattering. A rigorous treatment would of course require averaging of such a result over the full range of energetically allowed single-chain conformations (with proper Boltzmann weighting). Since even this treatment would not include proper account of concentration effects (sol concentration was ~2.4% w/w) the single-chain conformation estimate was considered adequate for present purposes.

So that the experimental agarose gel scattering could be modeled, it was in fact found necessary to assemble six double helices into the hexagonal rod form also shown in Figure 10 and to compute X-ray scattering appropriate to this structure over the angular range of relevance. This rod had a diameter of approximately 30 Å and, as Figure 12 makes clear, had a predicted SAXS curve closely similar to that already computed for a homogenous 30-Å diameter rod. Figure 12 shows how the calculated scattering from the hexagonal fiber model approaches the limiting value for the long 30-Å rod as the number of disaccharide res-

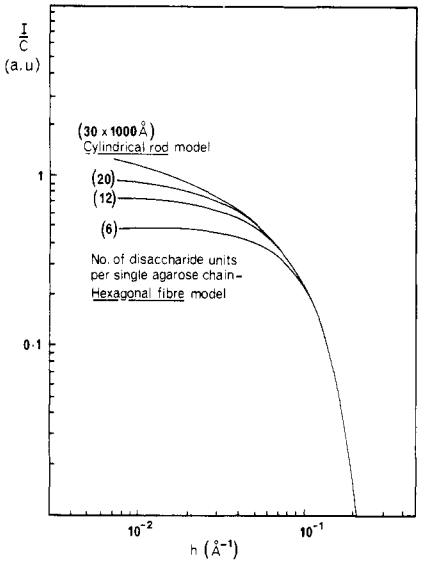

Figure 12. Calculated SAXS intensity (smeared) versus h curves for the hexagonal fiber structure as a function of increasing numbers of sugar residues per component polysaccharide chain. Previous scattering for the 30 × 1000 Å rod is included for comparison. The hexagonal fiber scattering approaches the rod scattering as the fiber length increases.

idues per component chain increases and the hexagonal fiber length increases. So that the experimental data could be modeled completely, however, i.e., to include scattering at the smallest available angles, scattering functions computed for higher aggregates based on the hexagonal fiber (equivalent to the earlier 90-Å rod component) would have to be added.

As has been noted previously, the modeling exercise just described does not conclusively determine the molecular structure of the fibers making up the agarose network, but it does provide an interesting and plausible suggestion as to how such aggregates could arise from the fiber diffraction helix. Accurate X-ray scattering data at somewhat larger h values would be required (i.e., between the current upper limit and those values corresponding to atomic resolution) to establish the model more securely. Then the hexagonal structure, if precise, might well be expected to give rise to subsidiary maxima in this h region (much as certain multisubunit proteins do[16]). Unfortunately, in the present case, the high-angle data carried much too high a noise level to be relied upon in this respect. Future experiments to pursue this point might employ a synchrotron source to measure the gel scattering as has been described recently in studies of scattering from an 11S soya globulin.[25]

Finally, it should be added that the current computation did not allow for any hydration of the fiber (internal to the helices or external), and this could make a contribution to the scattering from the real system. Even without this, however, the mass per unit length calculable for the unhydrated rod of Figure 10 ($\sim 1.0 \times 10^{-13}$ g cm^{-1}) is in good agreement with the low end of the range of experimental values ($(1.2\text{–}1.0) \times 10^{-13}$ g cm^{-1}) quoted earlier.

Discussion

The present work has confirmed two previously held views about the phenomenon of agarose thermoreversible gelation:

(1) The network is composed of substantial bundles of individual agarose chains, and there is a polydispersity of bundle thickness.

(2) The network strand assembly and disassembly processes follow different molecular pathways, i.e., there is a definite and irreducible hysteresis. This hysteresis has been shown to correspond to the requirement that conformational ordering of individual chains into helices must precede the formation of higher aggregates during the cooling cycle. However, the two steps that consist in the growth followed by the aggregation of helices cannot be separated experimentally. There is evidence arising from different agarose samples[3,7] that the aggregation process is always present. In other words, this implies that the double helix arrangement alone is not the stable configuration in solution at low temperatures. A lateral association of the dimers is also necessary, and this association, it appears, could involve a minimum of six double helices forming a basic cooperative unit, with larger aggregates of this unit also occurring. It should be added that despite this aggregation tendency, in the range of temperatures and concentrations and for the range of agarose samples investigated, no macroscopic precipitation is observed. It is also noteworthy that "melting out" of agarose gel network strands is a gradual process that can extend over a much greater temperature range and is not complete below 90 °C. Indeed, in connection with the setting-up and melting properties of agarose gels it is worth adding that recent work by Watase et al.[26] using rheological and differential scanning calorimetric (DSC) techniques provides a closely similar description of the agarose hysteresis property to that arrived at from the present studies. Young's modulus versus temperature curves and DSC endotherms provide a clear demonstration of the gradual melting out of gel network structure above 45 °C, and the DSC approach also confirms the much lower temperature of the more sharply defined gel-setting event. The current SAXS work also confirms that agarose in the hot solution state (particularly when autoclaved) is molecularly dispersed to the extent that it is reduced to single stranded coils, while in the gel the chains order and associate to produce at least two populations of bundle thickness. These populations are roughly equal in mass, but in number terms the thin bundles are much more abundant. A plausible model for the thin bundles can be constructed by using existing fiber diffraction data. This fits the current X-ray results and agrees well with other evidence such as previous estimates of fiber thickness and mass per unit length. The present description does also imply that melting of the network requires dissolution of strands of varying lengths and thicknesses as well as the additional breakdown of double helical entities, and this represents a broad spectrum of events and one which may be related to the observed spread of the "melting temperature". In any case heterogeneity at greater distance scales must be implied by the turbidity of agarose gels (see below).

As far as the network structure over a greater length scale is concerned, the present work has much less to contribute. The comparative independence of the form of gel scatter curves on agarose concentration and thermal history is at first surprising since the distribution of strand thicknesses ought to be sensitive to these factors and to produce different amounts of SAXS. However, the ordered thin strand may provide an explanation. Since most of the angular dependence of the experimental scattering arises from this source, it is perhaps less surprising that there is such a remarkable constancy. Changes in scattering corresponding to the formation of higher aggregates would be visible only at the smallest and least accessible angles. The relative masses of thick and thin species would be expected to vary significantly, however, so this cannot be the entire explanation. Perhaps it is more likely that there is a tendency for agarose gels to be phase separated

on a much larger scale than is measurable by the X-ray technique and for these phases to maintain a constancy of local network structure and local agarose concentration. The Pines and Prins work cited earlier appears to support this type of situation, though it must be said that little extra substantiation comes from such electron micrographs as are available or from our own optical microscopy.

Finally, the caveat must be issued that the results obtained here relate to one particular agarose sample, i.e., to one containing a particular degree of structural imperfection in relation to Figure 1 and one having a specific molecular weight distribution. Such factors can cause the extent of hysteresis behavior and other gel properties to vary from sample to sample, but in no way has the present work been able to systematically explore the scope of these variations.

Acknowledgment. We are grateful to our colleagues at the Unilever Research Laboratory, principally P. M. Hart and G. R. Atkins for their advice and assistance in the handling of agarose samples, and as always to L. A. Linger for preparation of the figures. We are also indebted to Drs. J.-P. Busnel and D. Durand of Université du Maine for help in characterizing agarose samples (molecular weight determination). M.D. acknowledges benefit of NATO sponsorship and of the Prix Langlois allocation and thanks the Biopolymer Research Group of Unilever Research Laboratory, Colworth House, for hospitality and support.

Registry No. Agarose, 9012-36-6.

References and Notes

(1) Araki, C. *Bull. Chem. Soc. Jpn.* **1956**, *29*, 543.
(2) Araki, C.; Arai, K. *Bull. Chem. Soc. Jpn.* **1967**, *40*, 1452.
(3) Arnott, S.; Fulmer, A.; Scott, W. E.; Dea, I. C. M.; Moorhouse, R.; Rees, D. A. *J. Mol. Biol.* **1974**, *90*, 269.
(4) Anderson, N. S.; Dolan, T. C. S.; Rees, D. A. *J. Chem. Soc. C.* **1968**, 569.
(5) Rees. D. A. *Chem. Ind.* **1972**, 630.
(6) Dea, I. C. M.; McKinnon, A. A.; Rees, D. A. *J. Mol. Biol.* **1972**, *68*, 153.
(7) Norton, I. T.; Goodall, D. M.; Austen, K. R. J.; Morris, E. R.; Rees, D. A. *Biopolymers* **1986**, *25*, 1009.
(8) Rees, D. A. *Adv. Carbohydr. Chem.* **1969**, *24*, 267.
(9) Rees, D. A. *J. Chem. Soc. B* **1970**, 877.
(10) Obrink, B. *J. Chromatogr.* **1968**, *37*, 329.
(11) Laurent, T. C. *Biochem. Biophys. Acta* **1967**, *136*, 199.
(12) Pines, E.; Prins, W. *Macromolecules* **1973**, *6*, 888.
(13) Miller, W. G.; Kou, L.; Tokyama, K.; Voltaggio, V. *J. Polym. Sci., Poly. Symp. Ed.* **1978**, *65*, 91.
(14) Clark, A. H.; Ross-Murphy, S. B. *Adv. Polym. Sci.* **1987**, *83*, 57.
(15) Busnel, J. P.; Durand, D. Université du Maine, 1987, private communication.
(16) Glatter, O.; Kratky, O. *Small-Angle X-ray Scattering*; Academic: London, 1982.
(17) Reference 16, Chapter 7.
(18) Morris, E. R.; Rees, D. A.; Welsh, E. J.; Dunfield, L. G.; Whittington, S. G. *J. Chem. Soc., Perkin Trans. 2* **1978**, 793.
(19) Amsterdam, A.; Er-el, Z.; Shaltiel, S. *Arch. Biochem. Biophys.* **1975**, *171*, 673.
(20) Coviello, T.; Kajiwara, K.; Burchard, W.; Dentini, M.; Crescenzi, V. *Macromolecules* **1986**, *19*, 2826.
(21) Yanaki, T.; Norisuye, T.; Fujita, H. *Macromolecules* **1980**, *13*, 1462.
(22) Guinier, A.; Fournet, G. *Small-Angle Scattering of X-rays*; Wiley: New York, 1955.
(23) Clark, A. H. Unilever Research, Bedford, U.K., 1987, private communication.
(24) Ter Meer, H.-U.; Burchard, W. In *Integration of Fundamental Polymer Science and Technology*; Kleintjens, L. A., Lemstra, P., Eds.; Elsevier Applied Science: Barking, U.K., 1985; p 230.
(25) Miles, M. J.; Morris, V. J.; Carroll, V.; Wright, D. J.; Bacon, J. R.; Nave, C. *Int. J. Biol. Macromol.* **1984**, *6*, 291.
(26) Watase, M.; Nishinari, K.; Clark, A. H.; Ross-Murphy, S. B., submitted for publication in *Macromolecules*.

Vibrational Spectroscopic Study on Molecular Deformation of Polydiacetylene Single Crystals: Stress and Temperature Dependences of Young's Modulus

Gang Wu, Kohji Tashiro, and Masamichi Kobayashi*

Department of Macromolecular Science, Faculty of Science, Osaka University, Toyonaka, Osaka 560, Japan. *Received July 23, 1987; Revised Manuscript Received March 3, 1988*

ABSTRACT: Resonance Raman and Fourier transform infrared absorption spectra of poly[1,6-di(*N*-carbazolyl)-2,4-hexadiyne] single crystals have been measured under tensile stress σ at various temperatures T, and the σ and T dependences of the vibrational frequencies have been measured for the skeletal modes. The peak positions of these bands were found to shift toward the lower frequency side as the stress increased: $\Delta\tilde{\nu}/\Delta\sigma = -40$ cm^{-1}/GPa for the C≡C stretching mode ν(C≡C), -31 cm^{-1}/GPa for ν(C—C), -5 cm^{-1}/GPa for ν(C═C), and -9 cm^{-1}/GPa for the ∠C—C═C bending mode δ(C—C═C) at room temperature. Such a tendency became more remarkable at higher temperature: $\Delta\tilde{\nu}/\Delta\sigma = -56$ cm^{-1}/GPa for ν(C≡C) and -20 cm^{-1}/GPa for δ(C—C═C) at 210 °C, respectively. By the normal coordinates calculation, variation of the intramolecular force constants with increasing applied stress has been estimated, and then Young's modulus E_l along the chain axis was calculated as a function of σ and T by the lattice dynamical theory. The E_l value calculated for $\sigma = 0$ GPa and $T = 300$ K is 41.1 GPa, in good agreement with the observed value 43.2 GPa. E_l was predicted by theory to exhibit about a 2% decrease per 1 GPa tensile stress at room temperature, while the observed decrement in E_l was about 4.6%/GPa. The calculated E_l was found to decrease by about 0.5% as the temperature increases from 27 to 210 °C, which is too small to reproduce the observed value of about 23.3%. The calculation of the atomic displacements and the potential energy distribution in the mechanically deformed polyDCHD chain showed that such a large discrepancy between the observed and calculated σ–T dependence of E_l was ascribed to the neglect of a significant contribution of such a vibrational mode as skeletal torsional motion, the band corresponding to this mode being hardly detected by the present FTIR and resonance Raman spectroscopy. The vibrational coupling between the resonant skeletal and off-resonant side-group modes was observed for some Raman bands, which was analyzed on the basis of the perturbation theory.

Introduction

In order to understand the mechanical properties of crystalline polymers from the molecular theoretical point of view, it is necessary to detect directly the changes in structure and intra- and intermolecular interactions induced by the externally applied stress and strain.

0024-9297/89/2222-0188$01.50/0